Local Buckling Behaviors of CFRP Sandwich Panels and Quasi-hyperboloidal One-way Shell

Yasutoshi TATEISHI* and Seishi YAMADA**

* M. of Eng., Shimizu Corporation, 4-17 Etchujima 3-Chome, Koto-ku, Tokyo 135-8530
** Dr. of Eng., Professor, Toyohashi University of Technology, 1-1, Tempaku-cho, Toyohashi-shi, Aichi Pref. 441-8580

Recently, FRP sandwich structures are applied in construction field such as bridge decks and large span roofs. These sandwich structures are constituted of FRP thin skins, foam core and thin ribs. About this type of sandwich panel, it was reported that local buckling occurred under in-plane compression and bending due to the large difference of stiffness between skin and core. The authors lead the analytical method of local buckling from energy principle in an effort to obtain the buckling stress conventionally. In this paper, first, the analytical method is introduced. Second, sandwich panel elements were examined under edgewise compression and bending to observe local buckling behaviors, and the experimental results were compared with the analytical values. Third, the quasi-hyperboloidal one-way shell was tested under three-points bending. The principle stress of skins from the experiment was compared with the FEM analysis and the proof load was predicted by the analytical method.

Key Words: CFRP, Sandwich Shell, Local Buckling, Experiment, Analytical Method

1. Introduction

The FRP (fiber reinforced polymer) sandwich panel structures are well known for light weight, high bending stiffness, high corrosion resistance, rapid installation, etc. In recent years, the applications of the FRP sandwich panels are increasing such as bridge decks[1] (Photo 1) and large span roofs for earthquake retrofits[2] (Photo 2). This sandwich structures are composed of CFRP thin skins, light weight foaming core and reinforced ribs. When the FRP sandwich panels are under compression and bending loads, the local buckling could occur due to the large difference of stiffness coefficient between face and core. The local buckling could cause decreasing the whole stiffness of the sandwich panel and ultimate destruction. Therefore the predictions of the local buckling load are very important for the safety and economical designs of FRP sandwich panels. The authors already presented the analytical method for local buckling of sandwich panels[3),4)].

In this paper, first, the analytical method is introduced. Second, sandwich panel elements are examined under edgewise compression and bending to observe local buckling behaviors, and the experimental results are compared with the analytical values. Third, the quasi-hyperboloidal one-way shell is tested under three-points bending. The principle stress of skins from the experiment is compared with the FEM analysis and the proof load is predicted by the analytical method.

Photo 1 Bridge Decks of Sandwich Panels made by Pultrusion and Injection Core (by Eric Munley)

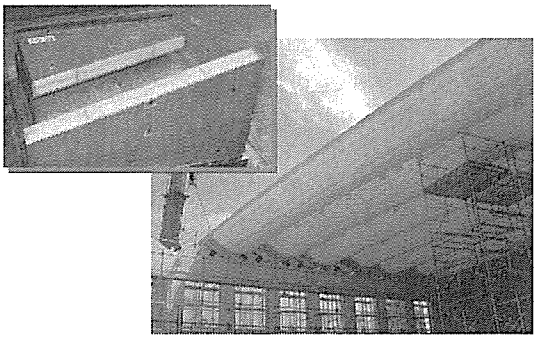

Photo 2 Section and Shells of CFRP Sandwich Panels made by VARTM

2. Analytical Method for Local Buckling

With regard to local buckling analyses of sandwich panel, Hoff's formulae[5] are well known. However, these formulae do not express the constraint effect of ribs. The authors presented the analytical method for local buckling including the constraint effect of latticed ribs[3),4)] from the stationary theorem of the total potential energy. This chapter introduces the analytical method.

2.1 Expressions of Local Buckling Stress

When the rectangular sandwich panels are under in-plane compressions, the four buckling modes (Fig.1) might be assumed, which are the independent mode (for thick core), the one-sided precedence mode (for out-of-plane bending load and imperfect case), the symmetric and the anti-symmetric modes (for thin core). The buckling stress of each mode is given as the following equation respectably. Herein, 'a' is half buckling wavelength along loading direction, 'b' half buckling wavelength along transverse direction.

$$\sigma_{cr} = \frac{D\pi^2}{t\,b^2}\left(\frac{a}{b}+\frac{b}{a}\right)^2 + \frac{2\sqrt{3}}{3\pi}\cdot\frac{\sqrt{{}^cE\,{}^cG}}{t}\,\frac{a}{b}\sqrt{a^2+b^2} \quad (1)$$

$$\sigma_{cr} = \frac{D\pi^2}{t\,b^2}\left(\frac{a}{b}+\frac{b}{a}\right)^2 + \left\{\frac{{}^cE}{{}^ch}\frac{a^2}{t\,\pi^2}+\frac{{}^cG\,{}^ch}{3t}\right\}\frac{a}{b}\left(\frac{a}{b}+\frac{b}{a}\right) \quad (2)$$

$$\sigma_{cr} = \frac{D\pi^2}{t\,b^2}\left(\frac{a}{b}+\frac{b}{a}\right)^2 + \left\{\frac{2\,{}^cE}{{}^cht}\frac{a^2}{\pi^2}+\frac{{}^cG\,{}^ch}{6t}\right\}\frac{a}{b}\left(\frac{a}{b}+\frac{b}{a}\right) \quad (3)$$

$$\sigma_{cr} = \frac{D\pi^2}{t\,b^2}\left(\frac{a}{b}+\frac{b}{a}\right)^2 + \frac{{}^cG\,{}^ch}{2t}\,\frac{a}{b}\left(\frac{a}{b}+\frac{b}{a}\right) \quad (4)$$

where bending stiffness $D=Et^3/12(1-\nu)$, E=Young's modulus of skin, ν=Poisson's ratio of skin, t = thickness of skin, ${}^cE$=Young's modulus of core, ${}^cG$=shear modulus of core, ${}^ch$ = thickness of core.

For the each equation, the first term is well-known buckling stress of simply supported rectangular plate under in-plane uniformly compression and the second term is the stiffening ingredient by core. These equations are decreasing functions for 'b', and have a minimum point for 'a'. Actually to obtain the minimum buckling stress, Newton Raphson method should be used for Eq.(1). As for the other equations, the minimum buckling stress should be obtained by 'a' of the local minimum point given by Eq.(6) , Eq.(7), Eq.(8).

$$a = \pi b\cdot\sqrt[4]{\frac{3D\,{}^ch}{3D\,{}^ch\,\pi^4+3\,{}^cE\,b^4+{}^cG\,{}^ch^2\pi^2b^2}} \quad (6)$$

$$a = \pi b\cdot\sqrt[4]{\frac{6D\,{}^ch}{6D\,{}^ch\,\pi^4+12\,{}^cE\,b^4+{}^cG\,{}^ch^2\pi^2b^2}} \quad (7)$$

$$a = b\cdot\sqrt[4]{\frac{2D\pi^2}{2D\pi^2+{}^cG\,{}^ch\,b^2}} \quad (8)$$

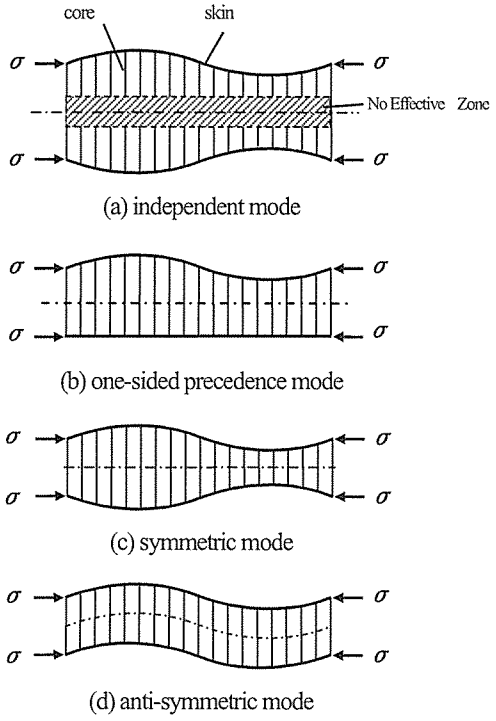

(a) independent mode

(b) one-sided precedence mode

(c) symmetric mode

(d) anti-symmetric mode

Fig.1 Local Buckling Modes

3. Specifications of CFRP Sandwich Panels

Table 1 shows the mechanical properties of the sandwich compositions for the experiments of this paper. The skin's material is CFRP ($_{CF}V_f$=5%, $_{GF}V_f$=45%), the core's material is phenol foam. There is large difference of stiffness coefficient between skin and core. It is generally known that phenol foam has brittle property. These components are made into one piece by vacuum assisted resin transfer molding (VARTM).

	Young's modulus (MPa)		shear modulus (MPa)	Poisson ratio
	E_L	E_T	G_{LT}	ν
Skin	30300	30300	5390	0.13
Rib	19600	12700	8160	0.42
Urethane Core	2.8		1.4	0.01
Phenol Core	6.6		3.3	0.01

4. Experiment of Sandwich Panel Elements

In this chapter, compression and bending tests for sandwich panel elements were conducted. The behavior of local buckling and the comparison with the analyses are described.

4.1 Specimen

Fig.1 is the specimen's shape for compression tests, and Fig.2 for bending tests. The thickness of the skin is 4mm for all specimens. The experimental parameters are core materials, core thicknesses, and rib pitches. There are 4 types specimens for compression tests, and 3 types for bending tests. The parameters and the number of the specimens are shown in Table 2.

Table 2 Experimental Parameters (Unit : mm)

Specimen Type	Load Type	Core Materials	Core Thickness	Rib Pitch	Specimen No.
EC-U100	Comp.	Urethan	100	400	2
EC-U75	Comp.	Urethan	75	400	7
EC-P100	Comp.	Phenol	100	450	3
EC-P100R	Comp.	Phenol	100	225	3
EOB-U75	Bend.	Urethan	75	400	3
EOB-P75	Bend.	Phenol	75	400	9
EOB-P75R	Bend.	Phenol	75	200	6

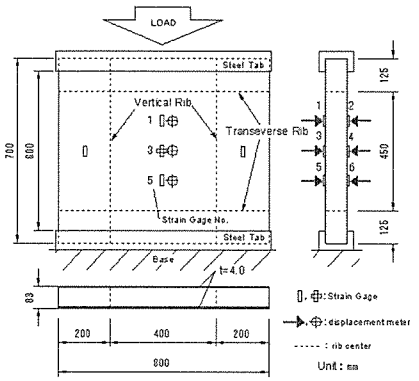

Fig.2 Shape of Specimen for Compression Tests

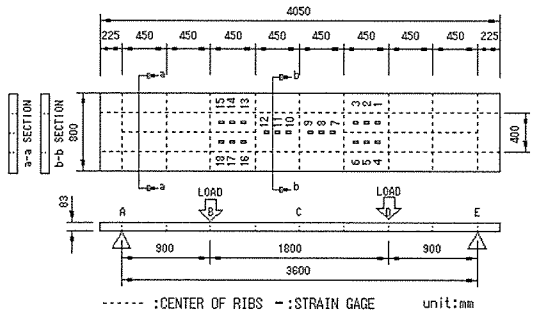

Fig.3 Shape of Specimen for Bending Tests

4.2 Loading and Measurement

The compression tests were loaded by Amsler type loading machine. The bending tests were loaded by two vertical jacks as for four points bending (Fig.2, Photo 2). The load and strain of the skins were measured.

4.3 Experimental Results

4.3.1 Load – Strain Relationship

Fig.4 shows the typical load - strain relationships. The local buckling point is defined at the strain reversal point on the curves. Fig.4(a) is the case of urethane core specimen under compression. It shows that the specimen has the remaining strength after the local buckling. Fig.4(b) is the case of phenol core specimen under compression. At this time, It shows that the specimen doesn't have the remaining strength. It is assumed to be due to the difference among the properties of the cores.

4.3.2 Local Buckling States

Photo 3 shows the local buckling states. Photo 3 is the case of urethane core specimen under compression; Photo 4 is the case of urethane core specimen under bending. It was possible to observe the buckling mode for urethane core specimens, but very difficult for phenol core specimens.

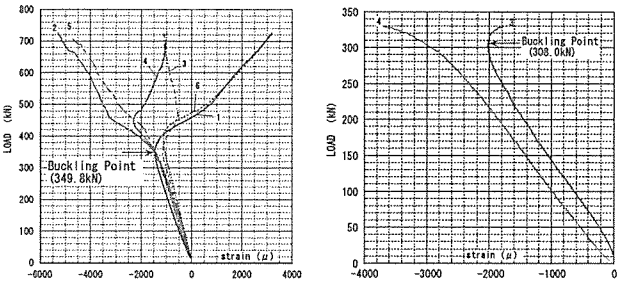

(a)EC-U75 (b)EC-P100

Fig.4 Load – Strain Relationships

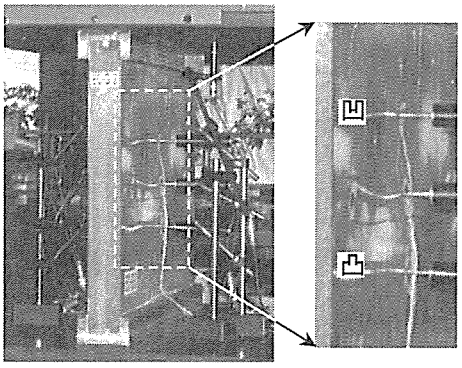

Photo 3 Local Buckling Figure
For Urethane Core Specimen Under Compression

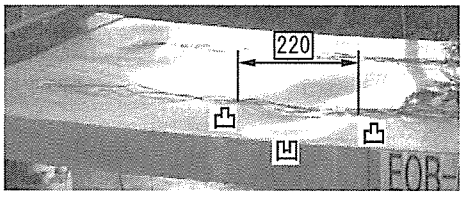

Photo 4 Local Buckling Figure
For Urethane Core Specimen Under Bending

4.4 Comparison with Analytical Results

Fig.5 shows the local buckling stress of the experiments and the analytical results. The experimental results are the average value for specimen types. The analytical results are calculated by Eq.(2). The analytical results are also indicated as the stress contributions. There are good agreements between the experimental results and the analytical results.

Fig.6 shows the relationships between buckling stress and half buckling wavelength which lead from the combination of Eq.(1) and Eq.(2). And it also shows the experimental data of each specimen. The diagram shows the good agreements between the experimental data and the analytical curves.

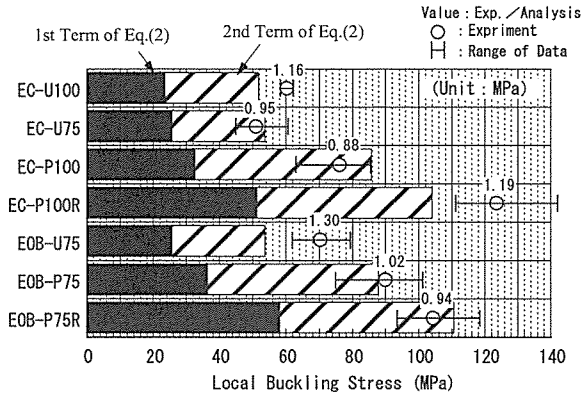

Fig.5 Comparison Between Average Experimental Results and Analysis For Local Buckling Stress

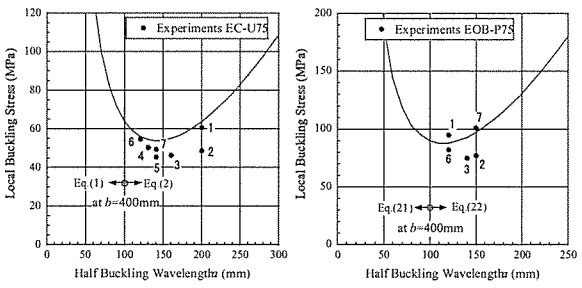

(a)EC-U75 (b)EOB-P75

Fig.6 Comparison Between Experimental Data and Analytical Curves

5. Experiment of Quasi-hyperboloidal One-way Shell

In this chapter, three points bending tests for quasi-hyperboloidal one-way sandwich shell were conducted. The behavior of local buckling and the comparison with the analyses are described.

5.1 Specimen

The shape of the specimen is shown in Fig.7 and Fig.8. Fig.7 shows the cross section. The standard thickness of the sandwich is 83mm, the standard thickness of the skin 4mm. This sandwich structure includes the latticed ribs of which the intervals are about 400mm for transverse direction and 450 mm for longitudinal direction.

Fig.8 shows the whole setting views. The shape is cut away from the hyperboloid and the longitudinal line has a large curvature radius. The testing span is 7,000 mm.

This large specimen was made into one piece by VARTM technique.

5.2 Loading and Measurement

The specimen was loaded under three points bending by the 6MN Amsler type loading machine (Fig.8, Photo 5). The load, displacements and strain of the skins were measured. The rosette gauges were set at the center of the each cellular skin in the quarter area of the specimen (Photo 5).

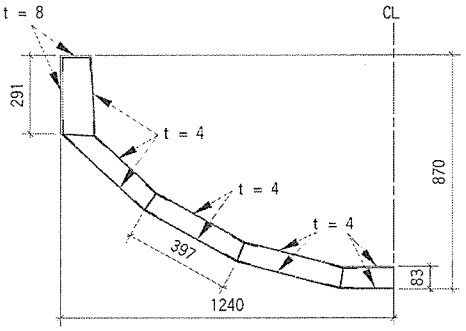

Fig.7 Cross Section

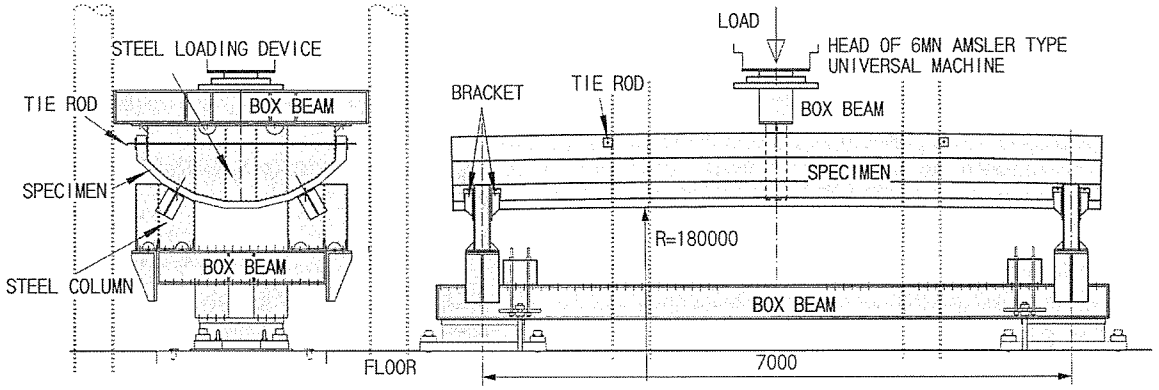

Fig.8 Specimen Figures and Loading Arrangement

5.3 Experimental Results

5.3.1 Load – Displacement Relationship

Fig.9 shows the relationship between load and perpendicular displacement at the center of the specimen. It is found that the relationship is almost linear till the ultimate load.

5.3.2 Load – Principal Stress Relationship

Fig.10 shows the relationship between load and principal stress of the skin where is at a rising edge cell near the loading device. The principal stress was calculated from the rosette gauges. The solid line is the minimum principal stress and the dash line the maximum one. The diagrams show that the relationship is almost linear till the ultimate load. The relations of the other cells show almost the same as Fig.9.

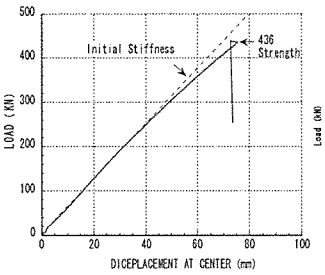

Fig.9 Load-Displacement

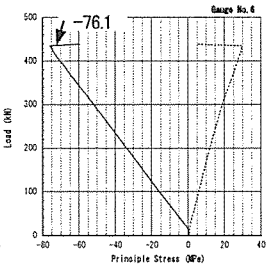

Fig.10 Load-Principle Stress

5.3.3 Principal Stress Vectors

Fig.11 shows the principal stress vectors which were calculated from the rosettes. It is found that the stress concentrated cells are the rising edge cells near the loading device. The absolute maximum value was 29.6 MPa.

5.3.4 Ultimate State

Photo 6 and Photo 7 show the ultimate state. Photo 6 is the outside of the rising edge and Photo 7 the inside one. Both figures show the progressions after local buckling of the skin. The ultimate strength is decided by the local buckling.

5.4 FE analyses

The finite element analyses, which are the linear stress analysis and linear buckling analysis, were carried out. The results from the FE analyses are compared with the experimental results.

5.4.1 FE Model

This is a quarter model about two axes of symmetry. As to the modeling of sandwich, Shell element is used for skin, Solid element is for rib and core. With regard to a mesh size of a sandwich cell, the core thickness is divided equally; skin is divided into three equal parts along the span direction and equally along the ridge direction. The 25 kN load, which means 100 kN as the whole model, is applied on the center nodes downward. The boundary conditions at support nodes are pin.

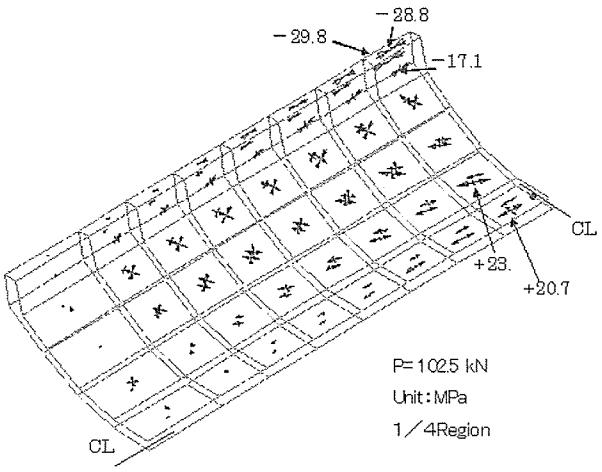

Fig.11 Experimental Results of Principal Stress Vectors

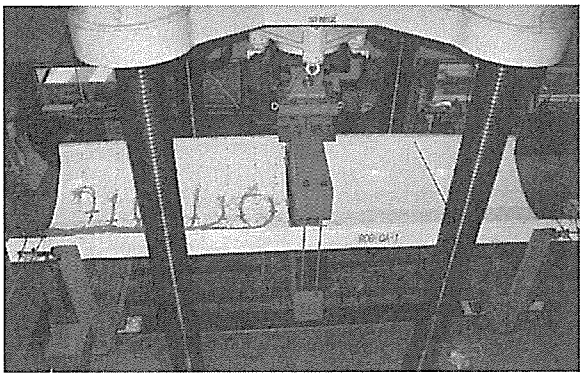

Photo 5 Whole View of Experiment
There are rosette gauges in a quarter region.

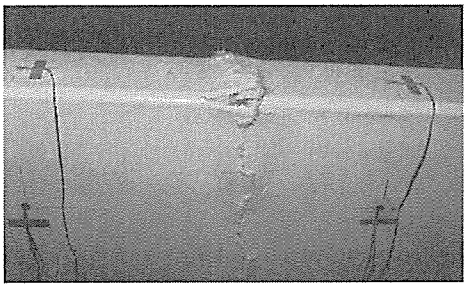

Photo 6 Ultimate State at Outside Rising Edge Cell

Photo 7 Ultimate State at Inside Rising Edge Cell

5.5 FE Results

5.5.1 Principal Stress Vectors

Fig.12 shows the principal stress vectors from the FEA. It is found that the stress concentrated cells are the rising edge cells near the loading device. When it compared to the experimental results of Fig.11, there are good agreements with the stress value and the directions of vectors. It is assumed to be due to the linearity of the experiment.

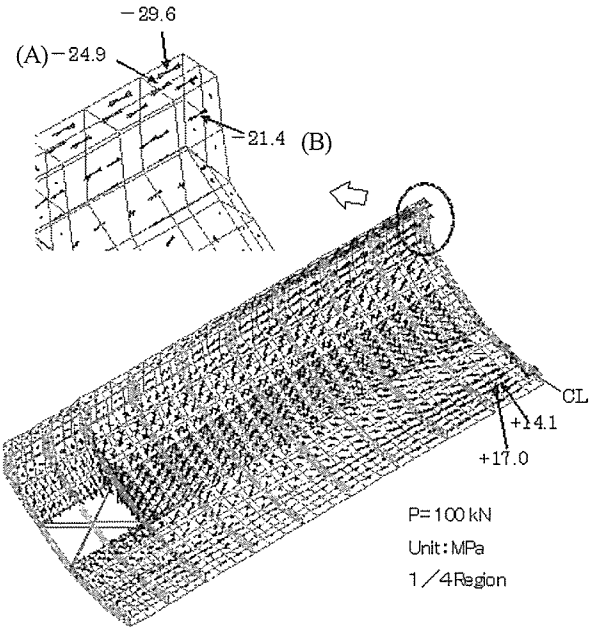

Fig.12 Principal Stress Vectors by EEA

5.6 Prediction of Buckling Load

When the rising edge cells seem to be under uniformly in-plane compression load or out-of-plane bending, the local buckling stress of the cells could be calculated from Eq.(2) (when the average core thickness is 107mm, the rib pitch is 291mm). Table 3 shows the local buckling stress of the rising edge cells near the loading device, which are shown as (A) and (B) in Fig.12. It is possible to predict the local buckling load by using the stress from the FEA at 100 kN load. Table 3 shows the predicted local buckling load. Fig.13 shows the prediction load and allowable design load on the experimental load – displacement diagram. It is possible to predict the local buckling load by applying the analytical method for local buckling of sandwich panel.

Table 3 Local Buckling Load by Analytical Method

Cell Position	Skin Thickness (mm)	FEM Stress At 100 kN (MPa)	Buckling Stress From Eq.(2) (MPa)	Predicted Buckling Load(kN)
(A)	8	21.4	95.4	446
(B)	4	24.9	92.3	371

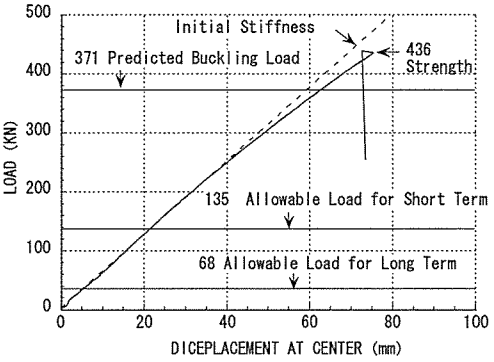

Fig.10 Experimental Load – Displacement Curve with Predicted Ultimate Load

6. Conclusions

- From the experimental results, the ultimate load is decided by the local buckling.
- The behaviors load – stress curve is depend on core materials.
- The results from the presented analytical method for local buckling has good agreement with the experimental results.
- The principle stress vectors of the sandwich skins fit to the results of the FEM stress analysis on the large span sandwich structure.
- It is possible to predict the ultimate buckling load by the presented analytical method to large span sandwich structures.

References

1) 'Advanced Materials', Structural Engineering International, IABSE, Vol.12, No.2, 2002

2) Tateishi, Y., Sugizaki, K., Fujisaki, T., Kanemitsu, T., and Yonemaru, K., Experiment and Application of CFRP Sandwich Panel, *CD-ROM Proc. IASS symp.,* NAGOYA, TP037, 2001

3) Tateishi, Y. and Yamada, S., Theory and Experiments of Local Buckling in CFRP Sandwich Panels, *CD-ROM Proc. IABSE symp.,* SHANGHAI, SHA223, 2004

4) Tateishi, Y. and Yamada, S., Comparisons between Theories and FE results about Local Buckling of CFRP Sandwich Panels, *CD-ROM Proc.* 9th Japan International SAMPE Symposium & Exhibition (JISSE-9), S7-12, 2005

5) Hoff N. J. and Mautner S. E., "The Buckling of Sandwich-Type Panels", *Journal of the Institute of Aeronautical Sciences*, Vol.12, No.3, pp285-297, July 1945